

Electron Spin Resonance Scanning Probe Spectroscopy for Ultrasensitive Biochemical Studies

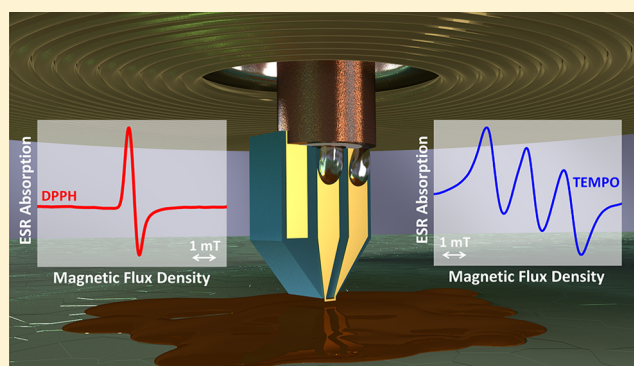
Jason P. Campbell,[†] Jason T. Ryan,[†] Pragya R. Shrestha,[†] Zhanglong Liu,^{†,‡} Canute Vaz,[†] Ji-Hong Kim,[†] Vasileia Georgiou,^{†,§} and Kin P. Cheung^{*,†}

[†]National Institute of Standards and Technology, 100 Bureau Drive, MS 8120, Gaithersburg, Maryland 20899, United States

[§]Department of Electrical and Computer Engineering, George Mason University, 4400 University Drive, Fairfax, Virginia 22030, United States

Supporting Information

ABSTRACT: Electron spin resonance (ESR) spectroscopy's affinity for detecting paramagnetic free radicals, or spins, has been increasingly employed to examine a large variety of biochemical interactions. Such paramagnetic species are broadly found in nature and can be intrinsic (defects in solid-state materials systems, electron/hole pairs, stable radicals in proteins) or, more often, purposefully introduced into the material of interest (doping/attachment of paramagnetic spin labels to biomolecules of interest). Using ESR to trace the reactionary path of paramagnetic spins or spin-active proxy molecules provides detailed information about the reaction's transient species and the label's local environment. For many biochemical systems, like those involving membrane proteins, synthesizing the necessary quantity of spin-labeled biomolecules (typically 50 pmol to 100 pmol) is quite challenging and often limits the possible biochemical reactions available for investigation. Quite simply, ESR is too insensitive. Here, we demonstrate an innovative approach that greatly enhances ESR's sensitivity (>20000× improvement) by developing a near-field, nonresonant, X-band ESR spectrometric method. Sensitivity improvement is confirmed via measurement of 140 amol of the most common nitroxide spin label in a ≈593 fL liquid cell at ambient temperature and pressure. This experimental approach eliminates many of the typical ESR sample restrictions imposed by conventional resonator-based ESR detection and renders the technique feasible for spatially resolved measurements on a wider variety of biochemical samples. Thus, our approach broadens the pool of possible biochemical and structural biology studies, as well as greatly enhances the analytical power of existing ESR applications.



Electron spin resonance (ESR) spectroscopy is one of the most attractive and powerful analytical tools because it specializes in detailed interrogations of free radicals and broken bonds in a vast array of systems.^{1–4} Although many recent ESR publications entail extremely challenging solid-state quantum information experiments,^{5–7} the overwhelming majority of ESR applications strive to unravel biochemical reactions, proteomic structures, and inorganic physical chemistry^{8–12} in ambient environmental conditions. ESR experiments that monitor and manipulate the lifetimes of naturally occurring free radicals or those that purposefully introduce extrinsic free radicals into molecules of interest have unraveled some of the most complex and confounding atomic-scale chemical and biological processes.^{12–15} Recently, ESR has been identified as particularly well-suited to determine smaller-scale dynamic and larger-scale conformational changes in protein structures not amenable to other methods (i.e., macromolecular X-ray crystallography and structural nuclear magnetic resonance spectroscopy).^{8,16,17} Despite this success, ESR is often, unfairly, viewed as a complementary or niche technique^{9,18–20} which requires extraordinary sample preparations to combat ESR's relative

insensitivity. In this work, we present an ESR methodology that greatly increases ESR sensitivity and unlocks the potential for ESR investigations on virtually any soft matter, or solid-state, material system.

ESR sensitivity is limited by an experimental arrangement which relies, quite heavily, on a microwave resonator to induce ESR transitions and subsequent detection.^{21,22} The resonator serves as an extremely low noise amplifier with sensitivity proportional to the quality factor and the ratio of resonator volume to sample volume or filling factor. However, it also introduces restrictions on sample shape, volume, concentration, and conductivity, which ultimately limits the minimum practical sensitivity to 50–100 pmol.¹⁴ Conventional ESR spectroscopy using a resonator thus relegates the technique almost entirely to bulk measurements (μL volumes) of spin ensembles.²³

To circumvent these resonator-derived experimental impediments, we have developed a method to excite and detect ESR

Received: February 4, 2015

Accepted: April 13, 2015

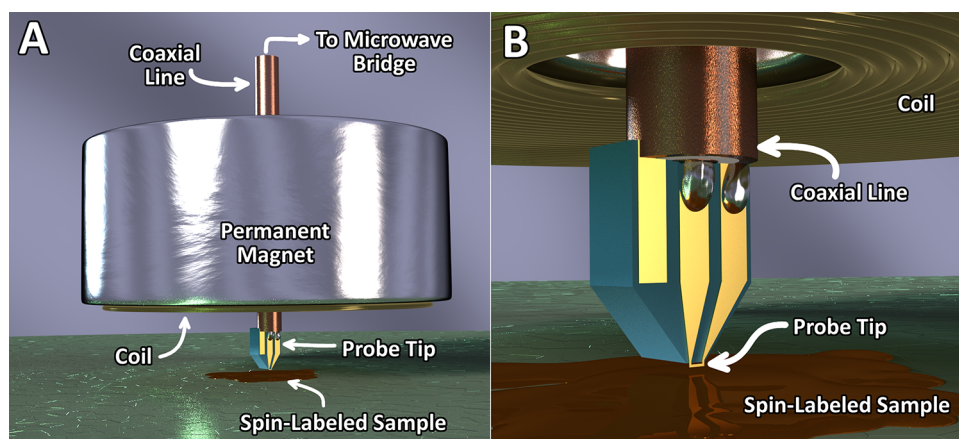


Figure 1. (A) Illustration of the experimental arrangement in which a nonresonant near-field “ESR-probe” is axially positioned through an annular shaped permanent magnet. This arrangement, (B), allows for an interrogation of virtually any spin-labeled sample brought into close proximity to the probe tip.

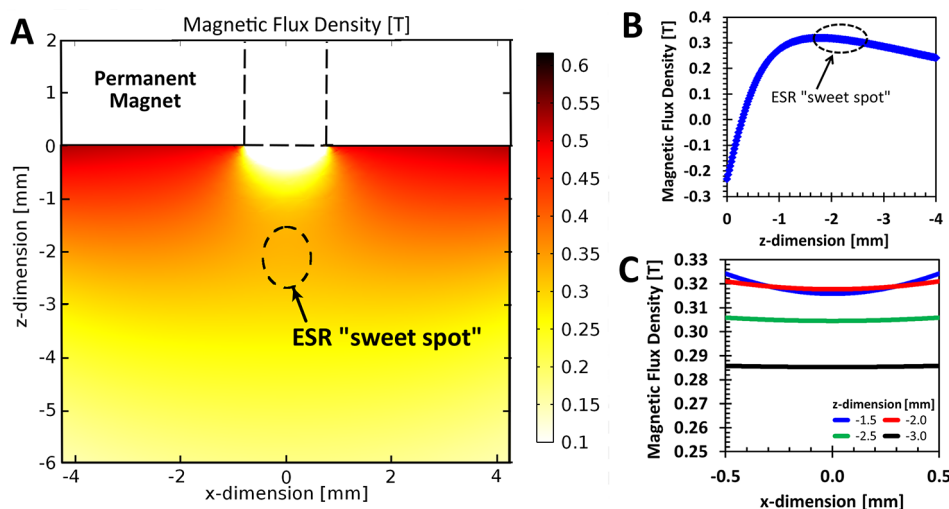


Figure 2. (A) Three-dimensional finite element calculation of the magnetic flux density in the region below the surface of the annular shaped permanent magnet. (B) Magnetic flux density calculation for an axial line centered on the inner hole of the magnet ($x = 0$ mm). In this figure, $z = 0$ mm corresponds to the magnet surface and $z < 0$ mm corresponds to the region below the magnet. (C) Further lateral dimension (x - y plane) calculations reveal acceptably small B_0 uniformity in the lateral directions.

transitions by using a nonresonant near-field microwave probe with a quality factor of ≈ 1 . The decrease in sensitivity due to the low quality factor is countered, in part, by an increase in the filling factor such that there is a net sensitivity improvement ($>20000\times$ better than commercial state of the art). Coupling this near-field microwave ESR probe with an appropriately designed small permanent magnet results in a highly sensitive ESR spectrometer that can be “scanned” across the surface of virtually any paramagnetic sample.

EXPERIMENTAL SECTION

Observation of ESR transitions requires that the sample of interest be simultaneously exposed to both a large quasi-DC magnetic field (B_0) and a comparatively smaller amplitude, typically microwave frequency, magnetic field (B_1). In a conventional ESR experiment, a large electromagnet supplies a uniform B_0 to the paramagnetic sample of interest and splits the energy of the spin system into two populations of unpaired spins that align either parallel or antiparallel to B_0 .^{21,22} A microwave source and waveguide resonator is used to simultaneously apply the B_1 field which provides the necessary

energy to promote “spin-flipping” transitions (parallel to antiparallel and vice versa). The parallel/antiparallel population difference results in a net absorption of energy which is detected using a highly sensitive microwave bridge. Each paramagnetic species, or spin-label, has a unique absorption criteria (B_0 and frequency of B_1) described by its g -factor. The g -factor is not only sensitive to the spin-label’s chemical and physical identity but also to local environment.

ESR observations, as described above, are accomplished with an elegant combination of a much smaller permanent magnet (B_0) and a nonresonant near-field ESR probe tip (B_1) as illustrated in Figure 1a,b.

Homogeneity, Stability, and Control of B_0 . An axially magnetized annular shaped NdFeB (neodymium) permanent magnet (outer diameter = 15.9 mm, inner diameter = 1.6 mm, and thickness = 7.9 mm) provides the necessary magnetic field (B_0) for X-band (≈ 9 GHz) ESR measurements (≈ 320 mT). Three-dimensional finite element calculations show, Figure 2a, that the annular magnet produces an ESR “sweet spot,” or optimal region 1.65–2.25 mm below the magnet surface along the center line. The region is both axially and laterally (x - y

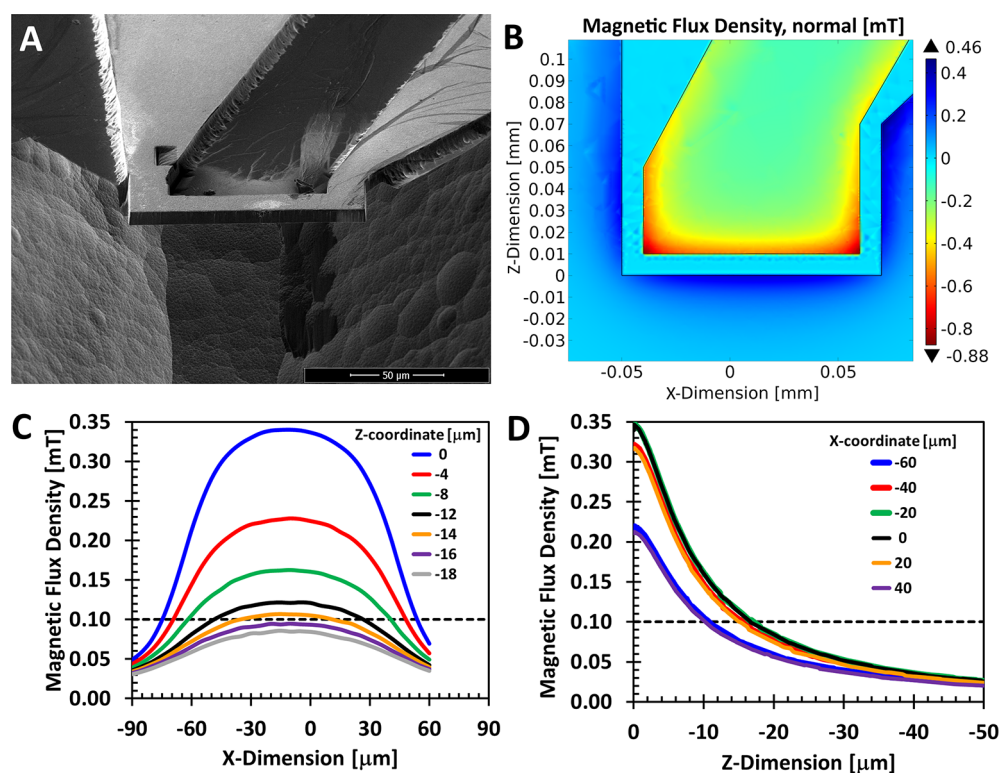


Figure 3. (A) Scanning electron micrograph of the ESR probe tip which consists of a cantilevered lithographically defined coaxial termination of arbitrarily small size. Three-dimensional finite element simulations (5 mW of input power) of the microwave magnetic field (B_1) surrounding the ESR probe tip termination, (B), defines the region probed. (C) Further calculation of the microwave magnetic flux density surrounding the ESR probe tip termination in the lateral dimensions. In the vertical dimension, (D), the magnetic flux density falls off with the inverse of the separation distance, as expected. The dashed lines in (C) and (D) are visual guides to help define the region, where $B_1 \geq 0.1$ mT.

plane) homogeneous in B_0 (see Figure 2b,c) over the comparatively smaller sample volume. This is experimentally confirmed by monitoring the ESR spectrum of a 2,2-diphenyl-1-picrylhydrazyl (DPPH) sample ($\approx 1000 \mu\text{m}^3$) affixed to the probe tip as the annular shaped magnet was stepped both laterally and vertically through the optimal region (not shown).

B_0 is both slowly varied (swept) by using a single-layer 40-turn coil of copper wire (coil inner diameter = 2 mm, coil outer-diameter = 10 mm) placed between the bottom of the permanent magnet surface and the optimum sample position. B_0 sweeping is accomplished via the application of a ramped current that is stabilized by current sensing feedback control which ensures that resistance variations due to Joule heating of the coil are compensated. In this manner, B_0 at the ESR probe tip can be swept ± 7 mT over a time scale ranging from 1 to 100 s. B_0 is also modulated at 100 kHz using this same 40-turn coil to facilitate phase-sensitive detection.

To minimize the coil/magnet heat transfer, a $200 \mu\text{m}$ air-gap is maintained between the bottom of the permanent magnet surface and the coil. Additional temperature control was achieved by embedding the annular shaped permanent magnet in a custom water-cooled heat sink, which allows magnet temperature control down to 0.1 K using an active closed-loop Peltier-driven water chiller. Temperature stability of the permanent magnet was experimentally verified by monitoring >250 consecutive measurements (≈ 1 h) of the ESR spectrum of a 2,2-diphenyl-1-picrylhydrazyl (DPPH) sample ($\approx 1000 \mu\text{m}^3$) affixed to the probe tip. The DPPH spectrum shift was $< 2 \mu\text{T}$ over these measurements.

Homogeneity, Stability, and Control of B_1 . The nonresonant near-field microwave probe consists of a non-magnetic semirigid coaxial cable (outer diameter = $508 \mu\text{m}$, length ≈ 127 mm) soldered to a lithographically defined overhanging aluminum/gold bilayer probe tip, Figure 3a (see Supporting Information for fabrication steps). The probe tip effectively short circuits the transmission line, leading to a maximum return current with near-zero electric field. This time varying current flow creates an enveloping microwave magnetic field (B_1). In the geometry depicted in Figure 3a, B_1 is oriented perpendicular to B_0 and extends into the plane of the sample under study. The overhanging probe tip used in this study has dimensions of $10 \mu\text{m} \times 10 \mu\text{m} \times 100 \mu\text{m}$, which were chosen for sample/probe tip positioning ease. This tip geometry could, of course, be scaled down to improve spatial resolution and enhance sensitivity. Although much smaller ESR probe sizes are experimentally accessible (Figure S1), positioning the probe tip above the sample surface (without crashing the tip) is challenging in the current configuration.

Since the sample is uniformly bathed in B_0 , the termination geometry and input microwave power define the spatial extent of the B_1 distribution and the consequent effective “ESR active region.” The coaxial line utilized in this system is capable of supporting up to 0.5 W, though our measurements typically utilize power levels in the range of 1–150 mW. Note that the power level can be arbitrarily decreased with a practical limit set by the noise of the microwave bridge detection circuit. We have comfortably performed ESR measurements with input power as low as 30 nW.

B_1 is examined with three-dimensional finite element calculations to determine the shape and extent of the ESR active region (Figure 3b). A profile of the lateral B_1 distribution is shown by plotting the magnetic flux density solution in the x -dimension for several positions in the z -dimension (Figure 3c). In general, B_1 is uniform in the x -dimension near the center of the probe tip. However, the lines leading to the probe tip (runners) cause the flux density to decrease near the probe tip edges. Assuming that we need $B_1 \geq 0.1$ mT to induce ESR transitions²¹ and that the probe tip can be positioned within 10 μm of the sample surface, the effective length of the probe tip (region where B_1 is sufficiently large to induce ESR transitions) is $\approx 2/3$ of the total length (≈ 65 μm in this case). A profile of the B_1 depth distribution is gained by plotting the magnetic flux density solution in the z -dimension for several positions in the x -dimension (Figure 3d). As expected, the microwave magnetic field falls off with the inverse of the separation distance. Since this work mainly focuses on surface measurements, the B_1 depth distribution is more than sufficient to probe through the relevant thickness. For this probe geometry, the 0.1 mT cutoff extends ≈ 15 μm from the bottom of the probe tip.

Microwave Bridge Detection. ESR induced absorption and dispersion of the microwaves at the near-field probe tip are sensed by using a highly balanced (10 nW/W) phase-sensitive microwave bridge (Figure S2). The input microwaves are split into a reference signal for local oscillator input of an X-band mixer and an input to the balanced bridge. The balanced bridge again splits the input into a reference and sample stimulating signals. Recombining the reference and sample signals completes the balanced bridge circuit. In the absence of ESR transitions, the reference signal is amplitude and phase adjusted (stepper motor control) to achieve destructive interference with the sample signal, thereby minimizing the bridge output. Once this “balance” is achieved, even very small ESR transitions introduce a signal above the bridge output noise floor and can be amplified and detected with the help of the X-band mixer and lock-in amplifier. The nonresonant near-field ESR probe paradigm, as described, allows for ESR detection at arbitrary frequencies (B_1), provided the appropriate magnetic field (B_0) is experimentally accessible. It also affords the freedom of more exotic fixed B_0 and swept microwave frequency detection with both B_0 modulation (Figure S3) as well as frequency modulation (Figure S4). We note that the advantages of frequency swept/modulated measurements^{24–26} are offset by degraded sensitivity due to the frequency dependence of the microwave bridge components. They are thus abandoned in favor of fixed frequency/swept B_0 measurements.

RESULTS AND DISCUSSION

Nonresonant, near-field ESR detection, as described above, is unaffected by many of the sample restrictions (volume, shape, conductivity) necessitated by conventional resonator-based spectrometers. Figure 4a qualitatively illustrates this situation with room temperature and atmospheric pressure, phase sensitive, continuous wave X-band ESR measurements for both liquid and solid phase spin label samples. A single droplet of ≈ 100 mmol/L 2,2,6,6-tetramethylpiperidine 1-oxyl (TEMPO) in ethylene glycol produces the expected spin-exchange broadened²² 3-line spectrum for this very common liquid phase nitroxide spin label. Several granules (≈ 1000 μm^3) of polycrystalline 2,2-diphenyl-1-picrylhydrazyl (DPPH) powder produce the expected spin-exchange narrowed²² single-line spectrum for this common solid-state spin reference. The total

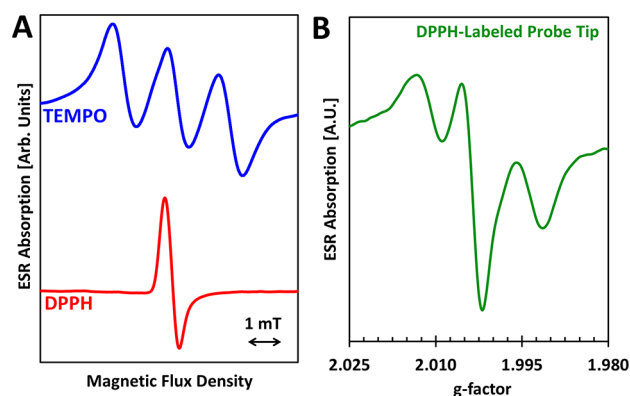


Figure 4. Ambient temperature and pressure ESR measurements, (A), of both liquid phase (TEMPO) and solid phase (DPPH) samples. The spectroscopic power of these measurements are demonstrated, (B), by measuring a TEMPO sample with a DPPH labeled ESR probe tip. The ESR spectra of (A) and (B) were acquired at nonsaturating microwave power and 100 kHz magnetic field modulation of ≈ 0.2 mT.

acquisition time for each spectra was 5 s. In both cases, these dissimilar samples were placed on a metallic sample holder positioned within the ESR active region. The sample holder-induced change in effective sample conductivity, which would normally prohibit conventional ESR detection,^{21,22} had no impact in nonresonant near-field ESR detection.

In general, ESR spectroscopic analysis involves relating an unknown spectrum from a sample of interest (a spin-labeled molecule) to a spectrum from a known reference sample.^{21,22} Knowledge of the reference sample's g -factor effectively calibrates the magnetic field experienced by the sample of interest^{21,22} and decodes the spin's local environment. Successful calibration requires that both samples experience the same B_0 . This experimental dictum is satisfied in our nonresonant near-field ESR spectrometer by affixing the reference sample directly to the microwave probe tip. In the spatial region encompassing the probe tip and the sample, B_0 uniformity is ≤ 600 nT/ μm of vertical displacement (see Figure 2) which easily satisfies the B_0 homogeneity requirement.²² Using this “spin-labeled” ESR probe tip to investigate a spin-labeled molecule of interest allows for full extraction of all the desired parameters.

Figure 4b qualitatively illustrates such an ambient temperature and pressure spectroscopic measurement in which the probe tip was spin-labeled with a (≈ 1000 μm^3) of DPPH crystal (electrostatically affixed to the probe tip) and positioned directly above a quartz microcapillary tube filled with the sample of interest (in this case a 50 mmol/L solution of TEMPO in ethylene glycol (Figure S5)). The microcapillary tube had an outer wall diameter of ≈ 8 μm and a wall thickness of ≈ 350 nm, verified by scanning electron microscopy images. The resultant ESR spectrum (Figure 4b) is, as expected, an overlap of both spectra in Figure 4a. By using the known DPPH g -factor of 2.0037 and the input frequency (8.845 GHz), the spectra can be plotted as a function of the g -factor, which fully calibrates this measurement.^{21,22} These calibrated spectra serve as proof that our ESR spectrometer is well suited to decode the local environment of spin labels in a wide variety of biochemical systems. This is a major asset for soft matter spin label studies¹⁴ as well as a variety of other solid-state measurements.⁴

The nonresonant near-field probe embodiment also presents the option of lateral scanning, similar to a scanned probe

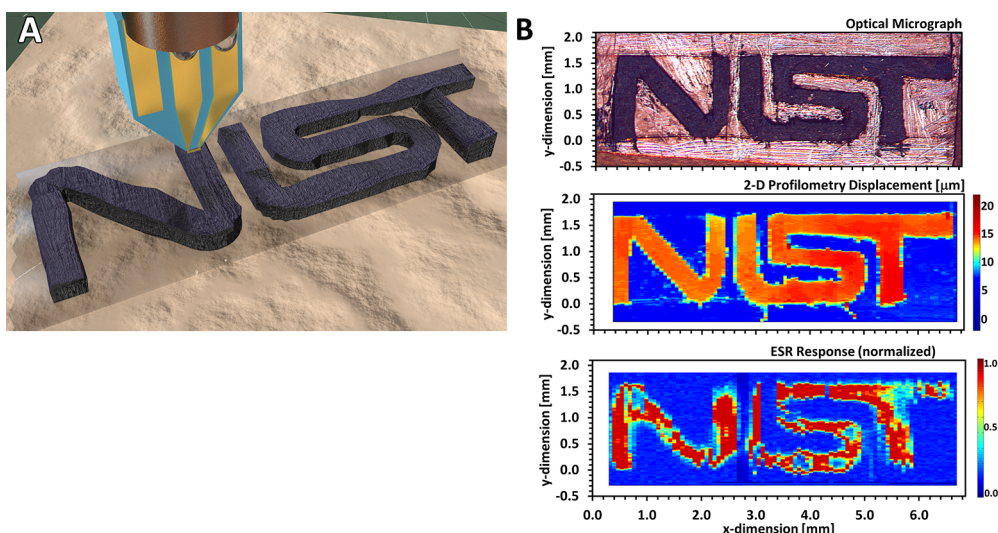


Figure 5. (A) ESR spatial profiling is accomplished by laterally scanning across a sample of patterned DPPH-labeled copy paper. ESR measurements were acquired at nonsaturating microwave power and 100 kHz magnetic field modulation of amplitude ≈ 0.2 mT. (B) Observed close correspondence between the optical micrograph, 2D profilometry, and ESR intensity map demonstrates the spatial profiling capability of this technique.

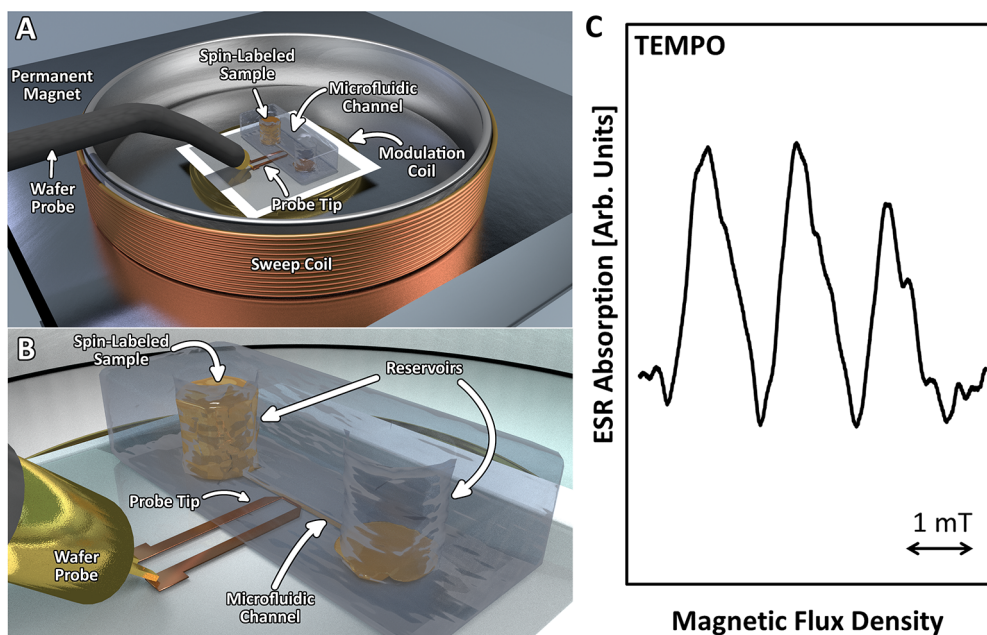


Figure 6. (A) Illustration of a second experimental arrangement more compatible with liquid phase ESR measurements as well as sensitivity calibrations. In this case, a lithographically defined ESR probe tip is defined on a glass substrate, (B), and microfluidic PDMS channel is placed on the ESR probe tip to provide a convenient liquid phase sample volume constraint. (C) ESR measurement of 593 fL of 1 mmol/L solution of TEMPO in ethylene glycol was acquired at nonsaturating microwave power levels and 100 kHz magnetic field modulation of amplitude ≈ 0.5 mT (≈ 30 min of signal averaging). In 1 h of signal averaging, we are able to resolve 140 amol of TEMPO with signal-to-noise ratio of three.

(Figure 5a). This capability was demonstrated by raster scanning across a patterned sheet of copy paper embedded with DPPH spin label. The pattern was appropriately sized, printed on copy paper, and affixed to a metal sheet using adhesive. The pattern was then cut out by hand with the aid of a microscope. A high concentration (>1 mol/L) of DPPH/acetone solution was prepared and carefully added to the copy paper pattern. The copy paper pattern absorbed the DPPH/acetone solution such that it was fully saturated. The pattern was then allowed to dry under ambient conditions. The acetone evaporated and the DPPH recrystallized such that there was a

high, relatively uniform, concentration of DPPH crystals embedded in the copy paper pattern. An optical micrograph, the corresponding 2D profilometry, and a continuous wave ESR signal intensity map are shown in Figure 5b. The DPPH spatial concentration was sufficiently high to allow ESR imaging with a constant probe tip to sample vertical offset of <1 μm and a lateral scan rate of <50 $\mu\text{m/s}$. The close correspondence between these images, including the within-pattern height variation, is an indicator of high quality ESR spatial resolution. The nonresonant near-field ESR imaging presented in this work is a true surface scanning probe with spatial resolution limited

only by the probe geometry. A geometrically scaled down ESR scanning probe could easily be employed to scan across a microfluidic array^{27,28} to investigate innumerable biomolecule interactions with extraordinary spectroscopic detail. It may be tempting to draw comparisons between a scaled down ESR probe tip and those used for scanning tunneling microscopy detected ESR efforts.^{29–32} However, the nonresonant near-field ESR probe does not require charge transfer between the tip and sample (no tunneling current). This further ensures that the approach described herein is sample agnostic.

As discussed above, conventional ESR sensitivity limits the potential application of this powerful analytical technique. The sensitivity gains associated with the nonresonant near-field ESR spectroscopic method circumvent these issues and open the window for ESR measurements on a much wider variety of biochemical systems. Sensitivity verification for this ESR spectrometer requires the placement of a known concentration of a well-defined volume of a spin standard in close proximity to the probe tip (within the active region). We demonstrated this objective by embedding the ESR probe tip within a microfluidic channel. The main elements of this embodiment are illustrated in Figure 6a,b. In this case, B_0 is supplied by a relatively large (10 cm \times 10 cm \times 5 cm) rectangular permanent magnet and is swept and modulated by using two separate coils (see Supporting Information). A 4 μm \times 0.8 μm \times 200 μm ESR probe tip is lithographically defined on a quartz substrate that is connected to the microwave bridge via a high-frequency shielded wafer probe in ground-signal configuration (see Supporting Information for fabrication steps). Placement of a polydimethylsiloxane (PDMS) microfluidic channel directly on the probe tip acts as a volume confinement mechanism to deliver an aliquot of the well-known TEMPO spin-label solution. Figure 6c illustrates the three-line nitroxide spin-label spectrum of a solution of 1 mmol/L TEMPO in ethylene glycol, which was loaded into the reservoir/channel via micropipette at ambient temperature and pressure. The channel volume (593 fL) was determined using profilometry of the channel as well as the probe tip (Figure S6). In ≈ 1 h of signal averaging, we are able to resolve 140 amol with a signal-to-noise ratio of 3 (see Supporting Information for sensitivity calculation). Since constricting the sample volume well within the probe active region artificially limits the ESR active region, the 140 amol observation should be taken as a worst-case sensitivity value; the actual sensitivity is very likely better. This particular experimental configuration (no spatial resolution but well-defined sample volume) was developed to illustrate sensitivity gains; however, there are clear merits to a (disposable) ESR probe tip/fluid cell capable of detecting spin-labeled biomolecules in solution.

The observed sensitivity improvement over conventional resonator-based ESR detection can be better understood by referring to the early work of Feher³³ who showed that the minimum number of observable paramagnetic spins is proportional to the ratio of the resonator volume, V_r , to the unloaded resonator quality factor, Q_{ur} . In comparison to a conventional X-band rectangular resonator ($V_r \approx 10 \text{ cm}^3$, $Q_{ur} \approx 10000$), the lithographically defined near-field nonresonant microwave probe used in the fluid cell experiment has an “effective” $V_c \approx 2.96 \times 10^{-10} \text{ cm}^3$ and $Q_{ur} \approx 1$). On the basis of these calculations, the geometric scaling represents a sensitivity improvement of about 6 orders of magnitude. The data shown in Figure 6c show a more modest sensitivity improvement. Our observation of a spin sensitivity of 140 amol corresponds to the

observation of $\approx 5.1 \times 10^6$ spins/0.1 mT, which, as discussed above, should be viewed as an upper boundary. However, this still represents remarkably favorable improvement ($>20000\times$ improvement) over conventional commercial rectangular resonator-based ESR detection (typically on the order of 10^{11} spins).^{22,34}

The disparity between the observed sensitivity improvement and the calculated sensitivity improvement is very likely due to nonideal optimization of the microwave bridge detection scheme, which is susceptible to temperature variation-induced phase shifts. We anticipate that scaling down the dimensions of the probe tip (decreasing the effective V_c) will further improve the sensitivity. The observed spin sensitivity is also comparable to many of the recent innovative planar resonator designs which often require special sample preparation and cryogenic temperatures.^{26,34–39} The minimal sample constraints and the ability to scan across paramagnetic surfaces at ambient conditions provides an advantageous methodology for interrogation of spin-labeled biological as well as solid-state samples.

ESR detection using a nonresonant near-field probe also has inherent advantages for pulsed-ESR measurements. Pulsed-ESR measurements are specifically well suited to study time dynamics of short-lived free radicals and protein dynamics and kinetics over very short (ms to ns) time scales.⁴⁰ In resonator-based pulsed-ESR spectrometers, the resonator quality factor is typically about 100, which introduces a proportional “dead time,” or capacitive time constant, immediately following the microwave pulse.⁴¹ This dead time interferes with the measurement of the fastest dynamic and kinetic processes. The nonresonant near-field probe, loaded quality factor ≈ 1 , drastically reduces the dead time and facilitates pulsed-ESR observations of time scales which are currently experimentally inaccessible. This effectively increases the spectroscopic content measured in each pulse and leads to more accurate measures of the biomolecule’s local environmental changes.

CONCLUSIONS

In conclusion, we have developed an innovative spatially resolved, highly sensitive, spectroscopic, nonresonant, near-field ESR detection scheme which is extremely well suited to study a vast array of biochemical reactions. The observed sensitivity improvement ($>20000\times$ greater than conventional ESR) allows for investigations of extremely small volumes (140 amol) of spin-labels/free radicals in biochemically relevant environments (solid or liquid phases at ambient temperatures and pressures). The ESR spectrometric method detailed in this work relies on an equipment set that is almost entirely commercially available with the few exceptions entailing very simple microfabrication and rudimentary machining. The relative ease of experimental assembly coupled with the demonstrated large sensitivity improvement presents an enormous opportunity to analytical chemistry and biological fields previously thought inaccessible to ESR investigations.

ASSOCIATED CONTENT

Supporting Information

ESR microwave probe tip fabrication steps, further detail on swept-frequency ESR measurements, the experimental arrangement for ESR measurements using a microfluidic channel, ESR probe tip on quartz substrates fabrication steps, PDMS fabrication steps, an extended discussion on ESR sensitivity

measurements. This material is available free of charge via the Internet at <http://pubs.acs.org>.

AUTHOR INFORMATION

Corresponding Author

*Phone: 301-975-3093. Fax: 301-975-8069. E-mail: kin.cheung@nist.gov.

Present Address

*Department of Chemistry, University of Florida, P.O. Box 117200, Gainesville, FL 32611, United States.

Notes

The authors declare no competing financial interest. The ESR methodology described herein is included in Patent Application US2014/0210473, filed April 3, 2014. The data discussed in this manuscript are contained entirely within the manuscript and Supporting Information.

ACKNOWLEDGMENTS

The authors thank V.A. Szalai of the Center for Nanoscale Science and Technology at NIST, and D.J. Gundlach of the Physical Measurements Laboratory at NIST for their careful review of this work. The authors acknowledge fruitful conversations with P.M. Lenahan of the Pennsylvania State University, J.W.F. Robertson, J.J. Kasianowicz, J. Geist, and D. Reyes-Hernandez of the Physical Measurements Laboratory at NIST, and R.G. Southwick, III of IBM.

REFERENCES

- (1) Columbus, L.; Hubbell, W. L. *Trends Biochem. Sci.* **2002**, *27*, 288–295.
- (2) Ikeya, M. *Nature* **1975**, *255*, 48–50.
- (3) Watanabe, T.; Yoshida, M.; Fujiwara, S.; Abe, K.; Onoe, A.; Hirota, M.; Igarashi, S. *Anal. Chem.* **1982**, *54*, 2470–2474.
- (4) Xiao, M.; Martin, I.; Yablonovitch, E.; Jiang, H. W. *Nature* **2004**, *430*, 435–439.
- (5) Pla, J. J.; Tan, K. Y.; Dehollain, J. P.; Lim, W. H.; Morton, J. J. L.; Jamieson, D. N.; Dzurak, A. S.; Morello, A. *Nature* **2012**, *489*, 541–545.
- (6) Rugar, D.; Budakian, R.; Mamin, H. J.; Chui, B. W. *Nature* **2004**, *430*, 329–332.
- (7) Wolfowicz, G.; Tyryshkin, A. M.; George, R. E.; Riemann, H.; Abrosimov, N. V.; Becker, P.; Pohl, H. J.; Thewalt, M. L. W.; Lyon, S. A.; Morton, J. J. L. *Nat. Nanotechnol.* **2013**, *8*, 561–564.
- (8) Altenbach, C.; Froncisz, W.; Hemker, R.; Mchaourab, H.; Hubbell, W. L. *Biophys. J.* **2005**, *89*, 2103–2112.
- (9) Barchasz, C.; Molton, F.; Duboc, C.; Lepretre, J. C.; Patoux, S.; Alloin, F. *Anal. Chem.* **2012**, *84*, 3973–3980.
- (10) Dockter, C.; Volkov, A.; Bauer, C.; Polyhach, Y.; Joly-Lopez, Z.; Jeschke, G.; Paulsen, H. *Proc. Natl. Acad. Sci. U.S.A.* **2009**, *106*, 18485–18490.
- (11) Gunderson, W. A.; Hernandez-Guzman, J.; Karr, J. W.; Sun, L.; Szalai, V. A.; Warncke, K. *J. Am. Chem. Soc.* **2012**, *134*, 18330–18337.
- (12) Oka, T.; Yamashita, S.; Midorikawa, M.; Saiki, S.; Muroya, Y.; Kamibayashi, M.; Yamashita, M.; Anzai, K.; Katsumura, Y. *Anal. Chem.* **2011**, *83*, 9600–9604.
- (13) Fanucci, G. E.; Cafiso, D. S. *Curr. Opin. Struct. Biol.* **2006**, *16*, 644–653.
- (14) Hubbell, W. L.; Cafiso, D. S.; Altenbach, C. *Nat. Struct. Biol.* **2000**, *7*, 735–739.
- (15) Koda, S.; Goodwin, J.; Khramtsov, V. V.; Fujii, H.; Hirata, H. *Anal. Chem.* **2012**, *84*, 3833–3837.
- (16) Fleissner, M. R.; Bridges, M. D.; Brooks, E. K.; Cascio, D.; Kalai, T.; Hideg, K.; Hubbell, W. L. *Proc. Natl. Acad. Sci. U.S.A.* **2011**, *108*, 16241–16246.
- (17) Kaminker, I.; Yagi, H.; Huber, T.; Feintuch, A.; Otting, G.; Goldfarb, D. *Phys. Chem. Chem. Phys.* **2012**, *14*, 4355–4358.
- (18) Gozen, I.; Jesorka, A. *Anal. Chem.* **2012**, *84*, 822–838.
- (19) Li, B. B.; Gutierrez, P. L.; Blough, N. V. *Anal. Chem.* **1997**, *69*, 4295–4302.
- (20) Stoyanovsky, D. A.; Melnikov, Z.; Cederbaum, A. I. *Anal. Chem.* **1999**, *71*, 715–721.
- (21) Poole, C. P. *Electron Spin Resonance; A Comprehensive Treatise on Experimental Techniques*; Interscience Publishers: New York, 1967.
- (22) Weil, J. A.; Bolton, J. R.; Wertz, J. E. *Electron Paramagnetic Resonance: Elementary Theory and Practical Applications*; Wiley: New York, 1994.
- (23) Hustedt, E. J.; Smirnov, A. I.; Laub, C. F.; Cobb, C. E.; Beth, A. H. *Biophys. J.* **1997**, *72*, 1861–1877.
- (24) Hirata, H.; Kuyama, T.; Ono, M.; Shimoyama, Y. *J. Magn. Reson.* **2003**, *164*, 233–241.
- (25) Jang, Z. H.; Suh, B. J.; Corti, M.; Cattaneo, L.; Hajny, D.; Borsa, F.; Luban, M. *Rev. Sci. Instrum.* **2008**, *79*, 046101.
- (26) Sakran, F.; Coptay, A.; Golosovsky, M.; Bontemps, N.; Davidov, D.; Frenkel, A. *Appl. Phys. Lett.* **2003**, *82*, 1479–1481.
- (27) Elvira, K. S.; Solvas, X. C. I.; Wootton, R. C. R.; deMello, A. J. *Nat. Chem.* **2013**, *5*, 905–915.
- (28) Tadmor, A. D.; Ottesen, E. A.; Leadbetter, J. R.; Phillips, R. *Science* **2011**, *333*, 58–62.
- (29) Balatsky, A. V.; Manassen, Y.; Salem, R. *Phys. Rev. B* **2002**, *66*, 195416.
- (30) Durkan, C.; Welland, M. E. *Appl. Phys. Lett.* **2002**, *80*, 458–460.
- (31) Heinrich, A. J.; Gupta, J. A.; Lutz, C. P.; Eigler, D. M. *Science* **2004**, *306*, 466–469.
- (32) Manassen, Y.; Hamers, R. J.; Demuth, J. E.; Castellano, A. J. *Phys. Rev. Lett.* **1989**, *62*, 2531–2534.
- (33) Feher, G. *Bell Syst. Tech. J.* **1957**, *36*, 449–484.
- (34) Narkowicz, R.; Suter, D.; Stonies, R. *J. Magn. Reson.* **2005**, *175*, 275–284.
- (35) Blank, A.; Dikarov, E.; Shklyar, R.; Twig, Y. *Phys. Lett. A* **2013**, *377*, 1937–1942.
- (36) Blank, A.; Suhovoy, E.; Halevy, R.; Shtirberg, L.; Harneit, W. *Phys. Chem. Chem. Phys.* **2009**, *11*, 6689–6699.
- (37) Malissa, H.; Schuster, D. I.; Tyryshkin, A. M.; Houck, A. A.; Lyon, S. A. *Rev. Sci. Instrum.* **2013**, *84*, 025116.
- (38) Shtirberg, L.; Twig, Y.; Dikarov, E.; Halevy, R.; Levit, M.; Blank, A. *Rev. Sci. Instrum.* **2011**, *82*, 043708.
- (39) Twig, Y.; Dikarov, E.; Hutchison, W. D.; Blank, A. *Rev. Sci. Instrum.* **2011**, *82*, 076105.
- (40) Jeschke, G. *Annu. Rev. Phys. Chem.* **2012**, *63*, 419–446.
- (41) Borbat, P. P.; Crepeau, R. H.; Freed, J. H. *J. Magn. Reson.* **1997**, *127*, 155–167.